

FEDSM2014-21659

**NONLINEAR MULTI-MODAL PANEL FLUTTER OSCILLATIONS
AT LOW SUPERSONIC SPEEDS**

Vasily Vedeneev

Department of Hydromechanics
Faculty of Mechanics and Mathematics
Lomonosov Moscow State University
Moscow, Russia 119991
Email: vasily@vedeneev.ru

Anastasia Shishaeva

Tesis LTD
18 Yunnatov str.
Moscow, Russia 127083
Email: nsh@tesis.com.ru

Konstantin Kuznetsov

Tesis LTD
18 Yunnatov str.
Moscow, Russia 127083
Email: kk@tesis.com.ru

Andrey Aksenov

Tesis LTD
18 Yunnatov str.
Moscow, Russia 127083
Email: andrey@tesis.com.ru

ABSTRACT

In this paper aeroelastic instability of a plate in a gas flow is investigated by direct time-domain numerical simulation. Plate deformation and gas flow are simulated in solid and fluid codes, respectively, with direct coupling between these codes. A series of simulations under different parameters has been conducted.

Three types of the plate response have been observed: stability, static divergence and flutter. Depending on Mach number, two types of flutter were detected: single mode flutter and coupled mode flutter. At $M = 1.8$, a good correlation between the present study and the piston theory for coupled mode flutter has been obtained. At lower M , from 1 to 1.6, single mode flutter in 1st, 2nd and higher modes has been observed. Amplitudes and frequencies of flutter limit cycle oscillations have been studied. It is shown that limit cycle oscillations can occur in form of pure one-mode oscillations, or include 1:2 internal resonance, when fluttering mode excites another mode. In the region of Mach numbers from 1.3 to 1.5, where several plate modes are simultaneously unstable, transition from periodic to quasi-chaotic flutter oscillations occurs.

INTRODUCTION

Aeroelastic instability of plates in a gas flow has been studied in many papers in context of panel flutter problem [1–5]. In case of subsonic flow the primary instability type is static (divergence), whereas in supersonic flow instability is oscillatory (flutter). Flutter instability in turn can be either coupled-mode flutter, or single-mode flutter. The first one occurs due to coalescence of eigenfrequencies; it has been studied in detail using aerodynamic "piston theory". The other flutter type, single mode flutter, occurs at lower flow speeds, and is studied insufficiently. In recent years detailed investigation of linear single mode flutter boundaries has been conducted [6,7], also this flutter type has been observed in experiments [8]. Unusual result that has been obtained is that there is a range of Mach numbers and plate lengths where several plate eigenmodes are unstable. Hence, when initial perturbation consisting of those modes is growing, formation of the limit cycle is governed by nonlinear interaction of the unstable eigenmodes.

Several time-domain simulations of nonlinear panel flutter were performed at conditions of transonic and low supersonic

speeds [9–11]. However, authors of the papers cited did not distinguish flutter type and did not investigate frequency spectra. From our point of view, analysis of spectrum, investigation of linear growth mechanism and of limit cycle type are extremely important due to different behaviour of flutter boundary and oscillation amplitude when changing the problem parameters. In particular, extrapolation of simulation results obtained for certain parameters to a wider parameter range is sensitive to flutter mechanism and structure of the limit cycle.

In this paper aeroelastic instability of a plate in a gas flow is investigated by direct time-domain numerical simulation. Plate and gas flow motion are modelled in solid and fluid codes, respectively, with direct coupling between them. The main goal of the paper is to investigate nonlinear development of growing oscillations in case of several growing eigenmodes.

Note that in contrast to studies [9–11], where the flow over one side of the panel was considered, we investigate the flow over both sides of the panel (Fig. 1). This, generally speaking, can yield different limit cycle oscillations due to difference in nonlinear aerodynamics. However, due to similar equations for linearized flow, stability boundaries coincide when comparing flow over both plate sides and over one side with two times higher flow density.

FORMULATION OF THE PROBLEM

We investigate motion of an elastic plate in a uniform air flow (Fig. 1). The problem is 2-dimensional. Unperturbed state of the plate is flat; the gas flows with a constant speed along both sides of the plate.

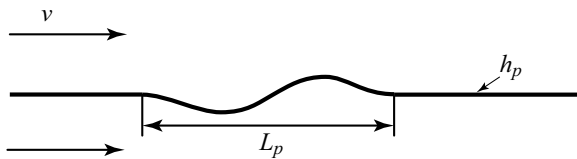


FIGURE 1. PLATE IN A GAS FLOW.

To simulate the plate motion, we use nonlinear Mindlin model, where elastic strains are calculated through Koiter-Sanders shell theory. The plate has dimensions 0.7×0.001 m and consists of three pieces: leading and trailing pieces are fixed, whereas the middle piece is free (Fig. 2). This is equivalent to considering only the middle piece of $L_p = 0.3$ m length and applying clamping boundary conditions $w(x, t) = \partial w(x, t) / \partial x = 0$ at its edges. Steel material properties were used in calculations: Young’s modulus $E = 2 \cdot 10^{11}$ Pa, Poisson’s coefficient $\nu = 0.3$, density $\rho_m = 7800$ kg/m³.

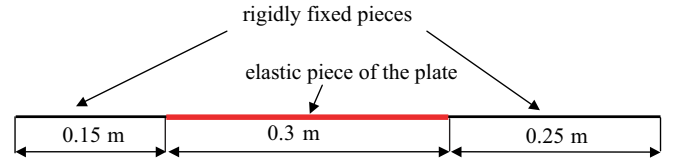


FIGURE 2. BOUNDARY CONDITIONS FOR THE PLATE.

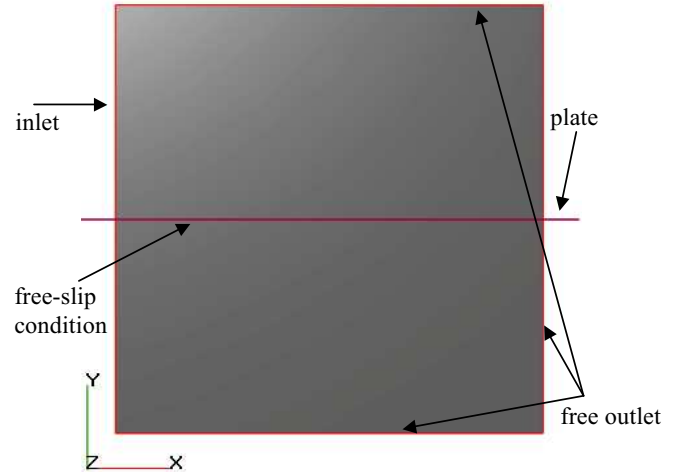


FIGURE 3. BOUNDARY CONDITIONS FOR THE GAS FLOW.

During a short initial time range $t = 0 \dots \varepsilon$, where $\varepsilon = 0.0002$ s, a slight disturbance force is applied to the panel in order to simulate initial perturbation of the system. At $t > \varepsilon$ no external force is applied to the plate or gas flow, so that behaviour of the system is governed by fluid-structure interaction only.

Simulation domain of the gas flow is square 0.6×0.6 m, which is shown in Fig. 3. The flow is viscous and is governed by Navier-Stokes equations for perfect gas. We neglect the boundary layer and investigate flutter in uniform flow, that is why instead of classical no-slip condition at the plate surface we assign free-slip condition: $v_n = v_p$, $\partial v_\tau / \partial n = 0$, where subscripts "n" and "τ" denote normal and tangent velocity components, v_p is the plate vertical velocity. This way we avoid formation of the boundary layer and do not need to excessively refine the mesh near the plate. In fact, this is equivalent to simulating flow of inviscid fluid; the reason why we did not use Euler equations directly is limitation of the aerodynamic code used to solve the problem.

Other boundary and initial conditions for the flow are as follows: we set uniform flow parameters at the inlet for any time t and homogeneous distribution of the same parameters over the simulation domain at $t = 0$ (initial condition). Temperature at inlet is equal to 273 K in all calculations. Two other flow parameters, namely, flow speed and density, are varied. Hereafter we will use two dimensionless parameters representing flow con-

dition: Mach number $M = v/a$ and dimensionless flow density $\mu = \rho/\rho_m$, where a is speed of sound, and ρ is the flow density. At the top, bottom, and aft domain boundaries condition of free flow outlet is assigned (Fig. 3).

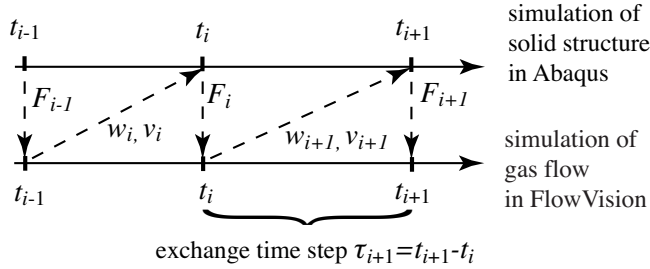


FIGURE 4. EXCHANGE ALGORITHM BETWEEN FLOWVISION AND ABAQUS.

METHOD OF SOLUTION

Analysis is conducted by using two coupled commercial codes. Plate motion is simulated in Abaqus, which is a widely used finite-element code oriented to stress analysis. The flow is simulated in FlowVision code developed by Tesis LTD, which uses finite volume method and is oriented to aero/hydrodynamic applications.

Interaction between the codes is organised through direct coupling mechanism along the surface of the deformed plate [12, 13]. Both codes are executed in turns; exchanges occur at each time step (generally not related to internal time steps of Abaqus and FlowVision) according to conventional serial staggered (CSS) procedure (Fig. 4). Each subsystem of equations (solid and fluid) is solved until the exchange time step is achieved, where results are sent to the other subsystem. Namely, displacements and velocities of the plate points are sent from Abaqus to FlowVision; pressure distribution along the plate surface is sent back from FlowVision to Abaqus. If the exchange time step coincides with each subsystem’s time step, then the scheme becomes explicit, even if each subsystem solver uses implicit numerical scheme. Generally, exchange time step, fluid solver time step and solid solver step can be different.

Mesh properties used in simulation are as follows. Abaqus plate model consists of hexagonal finite elements, 200 (length) \times 2 (through the plate thickness) mesh size. FlowVision flow model consists of 50 (length) \times 772 (height) finite volumes. Vertical finite volume dimension varies from 0.0001 m near the plate to 0.01 m far from the plate. A special mesh convergence study was performed (results are presented in the next section), which shows that the mesh is refined enough to obtain accurate limit cycle solution. When solving the problem with moving boundary,

FlowVision uses subgrid resolution technique [12] to capture the plate motion.

We use implicit Abaqus solver for structural motion, and set fixed time step 0.0001 s. If Abaqus-Flowvision exchange time point is achieved earlier than Abaqus simulation time at the next iteration, Abaqus step time is automatically reduced accordingly. FlowVision solver is also implicit; adaptive time step is based on maximum convective (=10) and surface (=1) Courant numbers. Abaqus-Flowvision exchange time step is equal to FlowVision time step.

Let us now observe results obtained at various flow conditions. It is convenient to analyze plate behavior after perturbation force applied by deflection A of a reference point plotted versus time. Reference point is located at 0.22 m downstream of the leading edge of the plate (Fig. 5). Fourier analysis was used to determine spectral components of limit cycles observed.

Three types of the plate behavior were observed: stability, divergence, and flutter. In the case of stability perturbed plate oscillates with rapidly decreasing amplitude and returns to the initial position. Reference point behavior is plotted in Fig. 6a. In the case of divergence (which was detected only for $M < 1$) plate also oscillates with decreasing amplitude, however, in contrast to stability, it is finally stabilizes in deflected position (Fig. 6b). In the case of flutter (which was observed only for $M \geq 1$) plate oscillation amplitude increases and then stabilizes at a non-zero value; the plate oscillates in a limit cycle (Fig. 6c).

CONVERGENCE STUDY

In order to ensure the numerical adequacy of the model we conducted a series of test simulations under the same physical parameters and different computational parameters: grid size and time steps, also we checked influence of disturbance force amplitude and its direction in order to make sure that instability is due to fluid-structure interaction and not because of numerical inaccuracies.

Shown in Fig. 7a are simulation results obtained on different grid sizes of the flow domain. It is seen that the limit cycle is the same in both cases. A small phase shift occurs due to slight difference in initial phase of oscillation growth. As the limit cycles almost coincide, we conclude that convergence in grid size

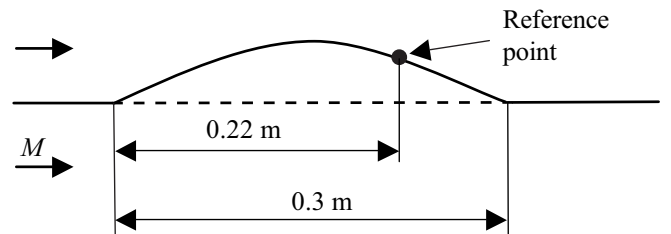


FIGURE 5. REFERENCE POINT LOCATION.

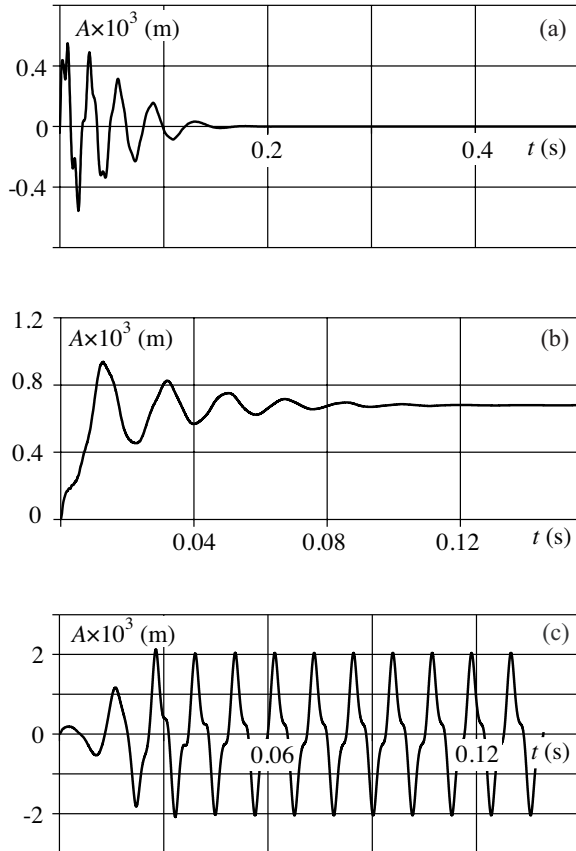


FIGURE 6. DEFLECTION OF THE REFERENCE POINT VS. TIME: STABILITY (a), DIVERGENCE (b), FLUTTER (c).

is achieved.

In Fig. 7b simulations with two time steps are shown. They correspond to Courant number (CFL) 2 and 10. Results almost coincide, which means that convergence in time step is achieved.

Shown in Fig. 8 are plate oscillations for different amplitudes of disturbance. Despite different initial phase of limit cycle formation, caused by different disturbance amplitude, in all cases the resulting limit cycle is the same. This proves that numerical model is adequate, and the limit cycle oscillations are cause by physical fluid-structure interaction. Also, calculations at different initial load directions were conducted. They showed that reverse of the perturbation load yields symmetrical panel oscillations, which also confirms correctness of the model.

RESULTS: OBSERVATION OF COUPLED MODE FLUTTER

We start analysis of obtained results with coupled mode flutter. This type of flutter occurs due to coalescence of two plate eigenfrequencies modified by the flow. Investigation of this flutter type is interesting due to two reasons. First, we watch ap-

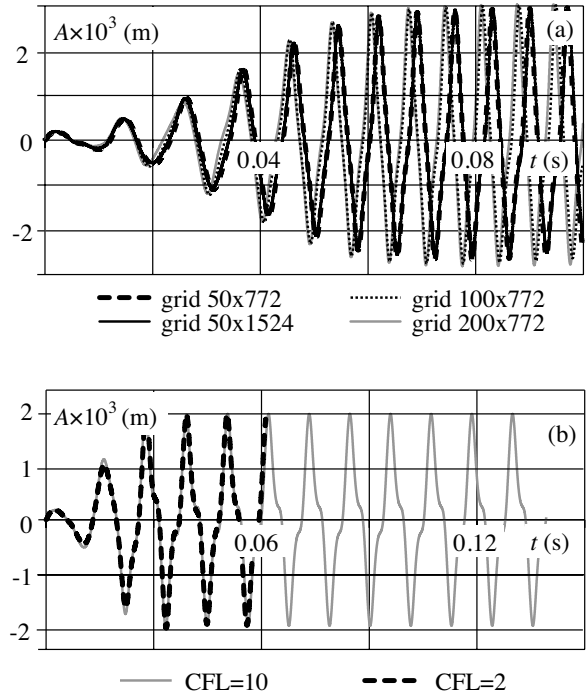


FIGURE 7. REFERENCE POINT DEFLECTION OBTAINED ON DIFFERENT GRIDS FOR $M = 1.15$, $\mu = 8.17 \cdot 10^{-5}$ (TOP); DEFLECTION OBTAINED WITH DIFFERENT TIME STEPS FOR $M = 1.06$, $\mu = 8.17 \cdot 10^{-5}$ (BOTTOM).

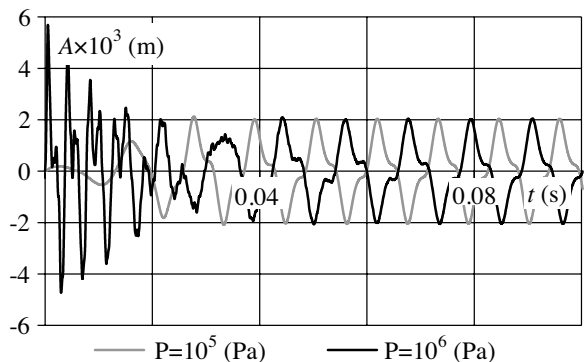


FIGURE 8. REFERENCE POINT DEFLECTION IN TIME FOR DIFFERENT PERTURBATION LOAD, $M = 1.06$, $\mu = 8.17 \cdot 10^{-5}$.

proaching and coalescence of eigenfrequencies while increasing Mach number, and occurrence of a limit cycle after the coalescence. Second, there are a lot of theoretical results obtained by using piston theory [1–3], and comparison of flutter boundary obtained in this study with classical results is one more independent test of the model.

We set Mach number $M = 1.82$ and vary dimensionless flow density μ in the range $1.5 \cdot 10^{-5} \leq \mu \leq 2.5 \cdot 10^{-4}$. These param-

eter values are chosen such that piston theory is still valid, and according to [1] coupled mode flutter should occur. Spectrum of the limit cycle should consist of one frequency located between the first and second natural frequency of the plate, that is why disturbance force that we applied contains both first and second natural plate modes.

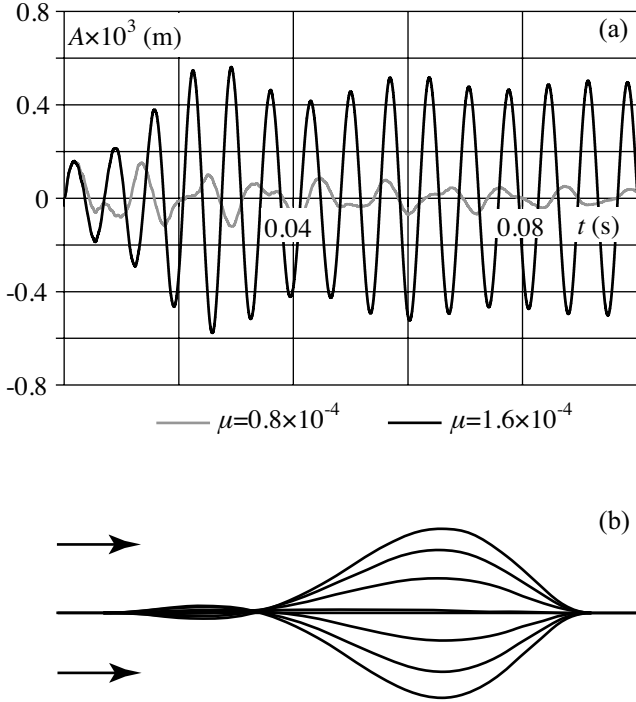


FIGURE 9. DEFLECTION OF THE REFERENCE POINT (a), OSCILLATION MODE SHAPE (b) IN CASE OF COUPLED MODE FLUTTER.

We obtained that when μ is not too large, plate oscillates with a small amplitude decreasing in time (Fig. 9a). Spectrum mostly consists of two frequencies. When increasing μ , the first frequency increases, while the second decreases, as shown in Fig. 10a. In this plot results of linear eigenfrequency calculation [7] are also plotted for comparison; it seen that the difference is negligible. At $\mu = \mu_{cr}$ the first and the second frequencies coalesce. At $\mu > \mu_{cr}$ only one frequency is detected in oscillation spectrum, which grows with increase of μ . Coalescence is accompanied by appearance of a limit cycle, whose amplitude increases with increase of μ (Fig. 10b). Oscillation mode shape is shown in Fig. 9b. It looks like a mixture of the first and second natural plate modes: it has a node located approximately at 1/4 plate length from the leading edge; amplitude of the rear part of the plate is much higher than that of the front part.

Critical dimensionless flow density (i.e. flutter boundary) obtained in simulation is $\mu_{cr} = 1.143 \cdot 10^{-4}$. Formula derived

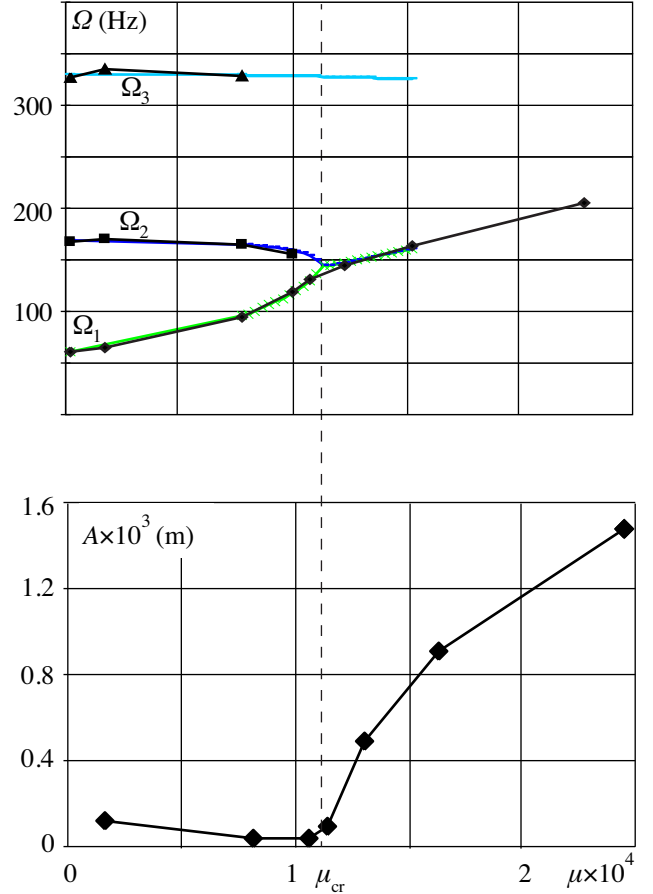


FIGURE 10. THE FIRST THREE EIGENFREQUENCIES (RESULTS OF THE PRESENT STUDY AND OF [7]) (TOP), OSCILLATION AMPLITUDE (BOTTOM) IN CASE OF COUPLED MODE FLUTTER.

through piston theory [3] gives the following criterion of coupled mode flutter:

$$\frac{M^2}{\sqrt{M^2 - 1}} > \frac{D_p}{a^2 \rho L_p^3} \lambda_{cr}, \quad (1)$$

where $D_p = Eh^3 / (12(1 - \nu^2))$ is the plate stiffness. Value of λ_{cr} depends on boundary conditions; for the plate clamped at both edges $\lambda_{cr} = 636$ [3]. Note that criterion (1) was obtained for gas flowing over one side of the panel, whereas in this simulation both plate sides contact the flow. Hence the flow density in (1) should be two times higher. Substitution of $M = 1.82$ and plate parameters into (1) yields $\mu_{cr} = 1.167 \cdot 10^{-4}$. This value is in less than 2% difference with the value obtained in simulation.

Therefore we conclude that coupled mode flutter boundary is correctly captured by the simulation. It is also seen that over-all coupled mode flutter properties, such as coalescence of eigen-

frequencies and LCO mode shape are correctly simulated. This provides additional verification of the model, and we can now proceed to results obtained for lower Mach numbers, which are the primary interest of this work.

RESULTS: OBSERVATION OF PANEL DIVERGENCE AND SINGLE MODE FLUTTER

For analysis of panel behavior at subsonic, transonic and low supersonic Mach numbers we fixed $\mu = 8.17 \cdot 10^{-5}$ and varied M from 0.7 to 2.0. This value of μ is small enough (compare with μ_{cr} from the previous section) to avoid any coalescence of eigenfrequencies, and hence coupled mode flutter.

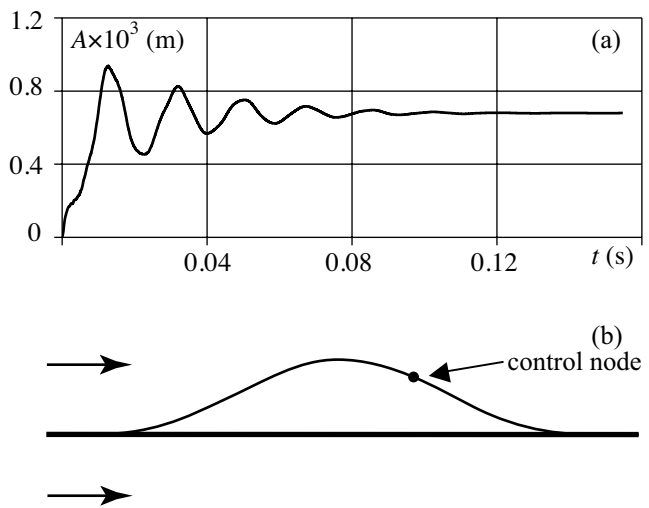


FIGURE 11. REFERENCE POINT DEFLECTION IN TIME (a), PLATE SHAPE (b) AT DIVERGENCE. $M = 0.909$.

For the parameters chosen the plate is stable for $M \leq 0.73$. At $M > 0.73$ perturbed plate makes several oscillations and stabilizes at a deformed state. Deflection of the reference point tends to a constant value as $t \rightarrow \infty$ (Fig. 11a). Shape of the diverged plate is very close to the first natural mode shape (Fig. 11b). Such a panel divergence was obtained in calculations for $M = 0.818, 0.909,$ and 0.969 .

Mach number $M = 1$ corresponds to a borderline state between divergence and single mode flutter. Plate oscillates with a frequency 23.5 Hz, which is more than twice lower than the first natural frequency, as plotted in Fig. 12a. In contrast to oscillations that occur at higher M , the plate motion is delayed in state of maximum and minimum deflection. The plate diverges upward and stays in this position some time. This delay can be considered as local stability of the diverged state of small duration. However, aerodynamic pressure at $M \approx 1$ cannot anymore

support the plate in static position, and the plate buckles to the opposite diverged state. In result oscillations are far from harmonic; in fact they consist of opposite divergence states changing each other. Oscillation mode shape looks like a traveling wave (Fig. 12b), exactly as predicted in [9].

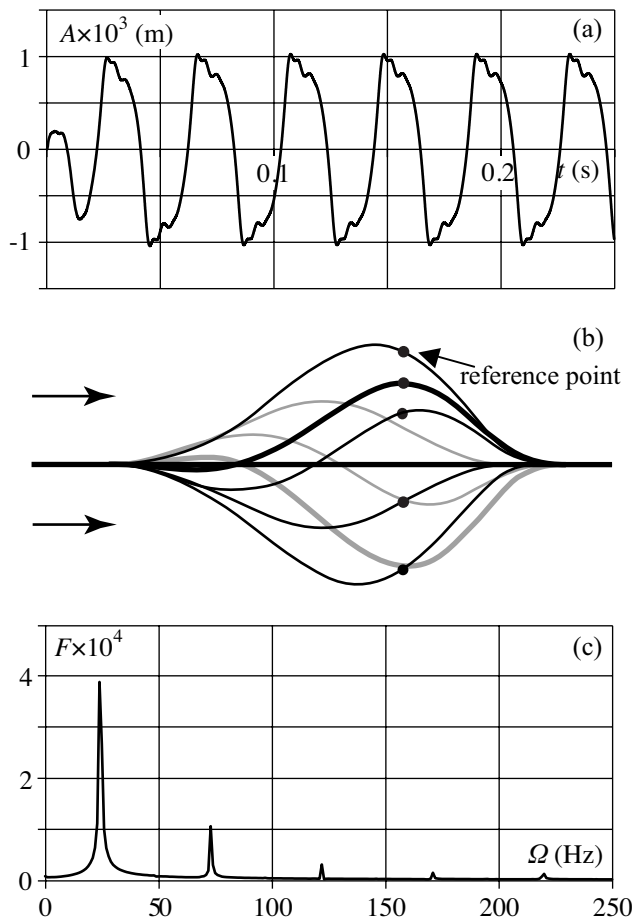


FIGURE 12. REFERENCE POINT DEFLECTION IN TIME (a), PLATE SHAPE (BLACK CURVES REPRESENT MOTION DOWN, GRAY CURVES REPRESENT MOTION UP) (b), SPECTRUM (c) AT $M = 1.0$.

Let us now proceed to $M > 1$. Note that smallness of the flow density excludes possibility of coupled mode flutter occurrence, therefore all oscillations that will be observed hereunder are caused by single mode flutter and nonlinear mode interaction.

In the range of Mach numbers $1.0 < M \leq 1.12$ we observed pure single mode flutter oscillations (Fig. 13). Plate shape looks close to the first natural mode shape; deflections of the plate upward and downward are symmetrical to each other. Oscillations have a certain component of travelling wave, however the more

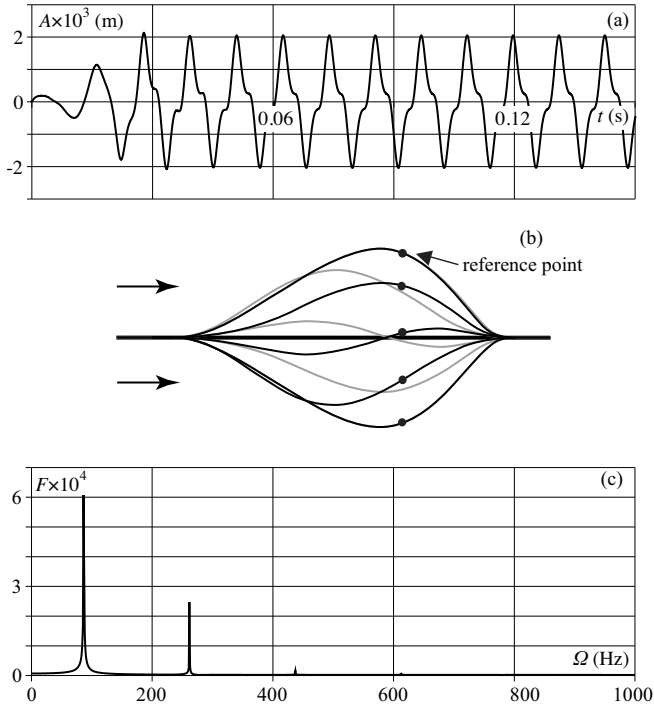


FIGURE 13. REFERENCE POINT DEFLECTION IN TIME (a) PLATE SHAPE (BLACK CURVES REPRESENT MOTION DOWN, GRAY CURVES REPRESENT MOTION UP) (b), SPECTRUM (c) AT SINGLE MODE FLUTTER. $M = 1.06$.

Mach number is, the more standing oscillation is. Spectrum of the reference point consists of two peaks being in ratio 1:3. The second peak is caused by a cubic nonlinearity of the plate and is not associated with a separate eigenmode.

In the range $1.12 < M < 1.33$ two types of limit cycle oscillations have been obtained. The first is a continuation of the symmetrical limit cycle from lower M . The second limit cycle is not symmetrical (Fig. 14). During the initial phase of oscillation growth the plate oscillates symmetrically, the mode shape is the same as in Fig. 13b. Starting from a moment when non-symmetry appears, growth of the second natural mode is clearly seen in oscillation shape (Fig. 14b). Oscillations are standing; no travelling wave component is present. Also, one more peak appears in oscillation spectrum, which is in 1:2 ratio with the frequency of the first peak. We conclude that growth of the second natural mode and non-symmetry of oscillations is caused by internal 1:2 resonance between the first and the second modes. Note that possibility of such a limit cycle that includes internal resonance was analytically proved in [14].

For the value of Mach number $M = 1.33$, high-frequency limit cycles were observed. This case apparently is a borderline between 1:2 resonant oscillations and quasi-chaotic oscillations described below.

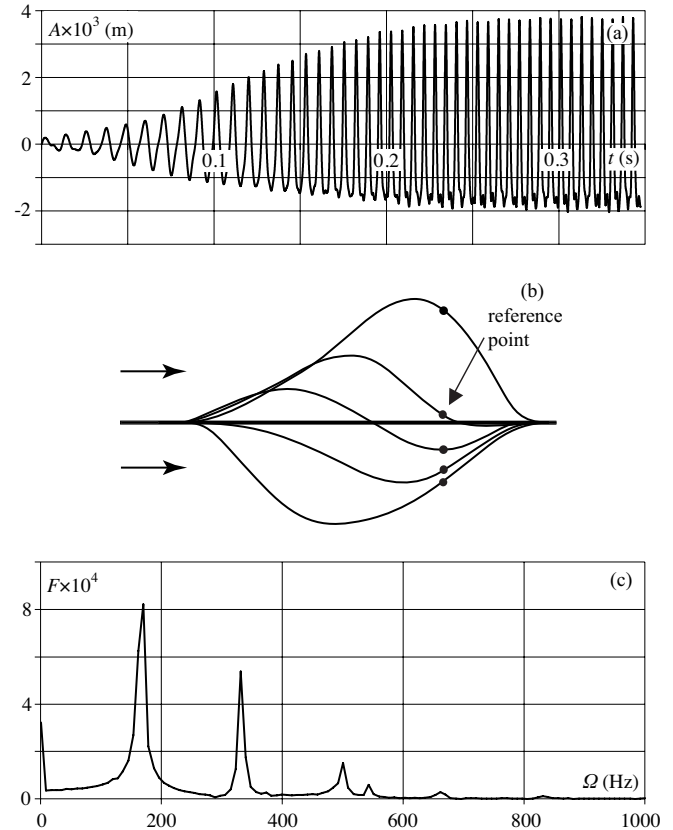


FIGURE 14. EXAMPLE OF REFERENCE POINT DEFLECTION IN TIME (a) PLATE SHAPE (VERTICAL SCALE 50:1) (b) AND FOURIER DIAGRAM (c) UNDER THE FLUTTER WITH INTERNAL RESONANCE. $M = 1.3$.

In the range of Mach numbers $1.36 \leq M < 1.42$ oscillation process dramatically changes (Fig. 15). Initially the plate oscillates in the first mode, later the second mode appears due to 1:2 resonance, as described above. However, little by little perturbations in form of third, fourth and fifth mode shapes appear. In contrast to the first and second mode, oscillations in higher modes are not periodic. Though for $M = 1.33$ such oscillations yield high-frequency limit cycle, for higher M this is not the case. Due to nonlinear mode interaction oscillations in the first and second modes lose periodicity and all the process becomes chaotic-like, with no specific mode dominated.

However, these oscillations are not "fully" chaotic. Indeed, according to [15], there are four criteria that must be satisfied to consider the process as truly chaotic:

1. Chaotic-like overall behaviour
2. Presence of wide frequency bands in the spectrum
3. Decrease of the autocorrelation function
4. Poincaré section consists of points filling an open set of the space

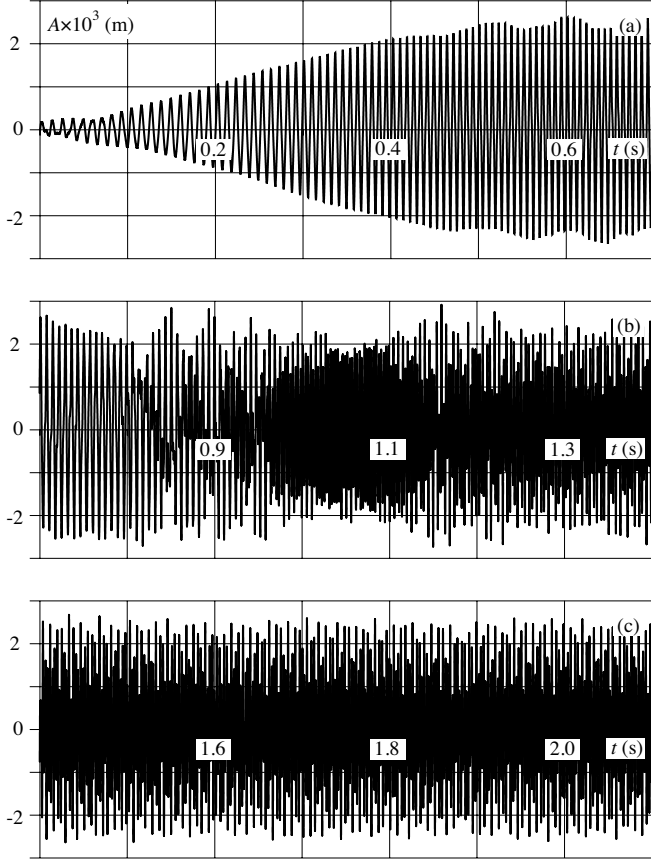


FIGURE 15. OSCILLATION PROCESS AND TRANSITION FROM LIMIT CYCLE TO QUASI-CHAOTIC HIGH-FREQUENCY OSCILLATIONS FOR $M = 1.39$. (a) DEVELOPMENT OF A LIMIT CYCLE, $t = 0..0.7$ s; (b) TRANSITION TO HIGH-FREQUENCY OSCILLATIONS, $t = 0.7..1.4$ s; (c) DEVELOPED HIGH-FREQUENCY NON-PERIODIC OSCILLATIONS, $t = 1.4..2.1$ s.

Consider the first three criteria in series. A close-up view of the resulting chaotic-like oscillations is shown in Fig. 16a; no periodicity of the reference point deflection is detected. Plate shapes captured at different moments of time are shown in Fig. 16b; it is seen that there is no apparent regularity of the shapes: they include all mode shapes from the first to the seventh. Video of the oscillation process clearly shows a non-regular motion of the plate.

However, the second criterion shows essential regularity of the spectrum, which is shown in Fig. 16c. As well as for single mode and resonant limit cycles, it consists of several clear peaks, which mean that the oscillations mostly consist of several single-frequency components. However, in contrast to previous cases, their frequencies are not in a simple ratio. Namely, two dominating frequencies are $f_3 = 371$ and $f_4 = 603$ Hz, which is

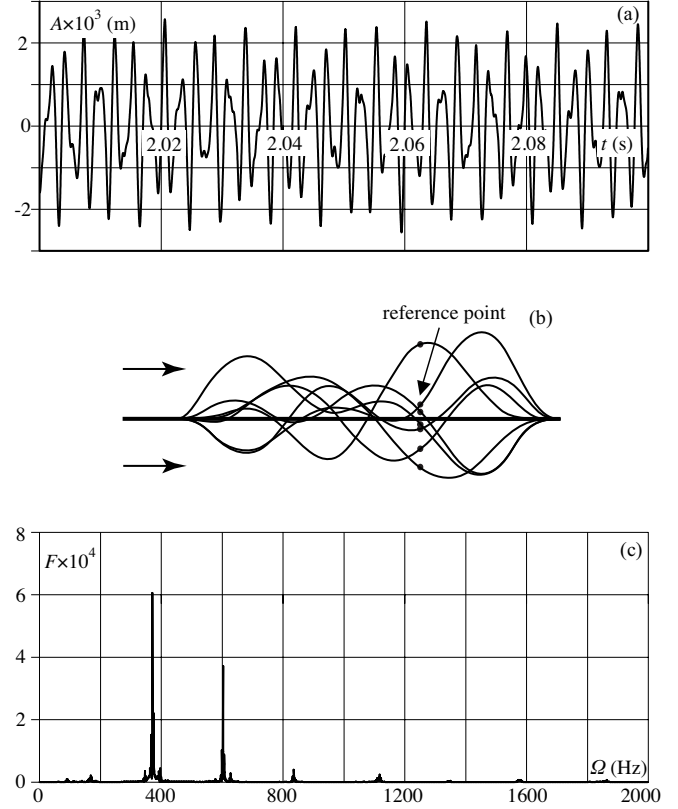


FIGURE 16. REFERENCE POINT DEFLECTION (CLOSE-UP VIEW OF THE FIGURE 15) (a), PLATE SHAPE (VERTICAL SCALE 30:1) (b), OSCILLATION SPECTRUM (C). $M = 1.39$.

in 8:13 ratio. This means that the attractor has a significant 8:13 internal resonance component. Though lower peaks, $f_1 = 89$ and $f_2 = 168$, have much less amplitude, they are present, and relate to the two dominating peaks at other ratios. Namely, $f_1 : f_3 \approx 6 : 25$, $f_2 : f_3 \approx 5 : 11$. Higher frequency peaks, $f_5 = 835$, $f_6 = 1117$, $f_7 = 1340$, $f_8 = 1573$, and $f_9 = 1863$ Hz, are the derivatives of the dominating ones due to cubic nonlinearity of the plate: $f_5 = 2f_4 - f_3$, $f_6 = 3f_3$, $f_7 = 2f_3 + f_4$, $f_8 = 2f_4 + f_3$, $f_9 = 5f_3$.

Let us now consider the third criterion. We define the auto-correlation function as follows:

$$F(\tau) = \lim_{t_1 \rightarrow \infty} \frac{\int_{t_0+\tau}^{t_1} \hat{A}(t) \hat{A}(t-\tau) dt}{\int_{t_0+\tau}^{t_1} \hat{A}^2(t) dt}, \quad (2)$$

where $\hat{A}(t)$ is the centred function $A(t)$:

$$\hat{A}(t) = A(t) - \frac{1}{t_1 - t_0} \int_{t_0}^{t_1} A(t) dt.$$

Denominator in the fraction (2) is taken for normalisation so that $F(0) = 1$. For periodic process the autocorrelation function is also periodic, whereas for a truly chaotic process it should be a decreasing function of τ . As the function $A(t)$ can be numerically obtained only for a limited range of times, we did not take the limit as $t_1 \rightarrow \infty$ and specified t_1 to be the last time for which $A(t)$ was calculated. As the integration period is limited, we calculated the autocorrelation function up to $\tau = (t_1 - t_0)/2$. In order to consider only quasi-chaotic part of oscillations, we specified $t_0 = 1.64$, and $t_1 = 2.64$ s. Resulting autocorrelation function is not decreasing so that the oscillations cannot be considered as truly chaotic.

On the other hand, the fourth criterion is satisfied, i.e. Poincaré section fills a full segment. This means that the attractor is not a "pure" limit cycle, as could be thought from the spectral and autocorrelation function criteria. Apparently, it actually has a dominating regular limit cycle component and a small quasi-chaotic component.

When Mach number is increased more, chaotic-like oscillations disappear. Surprisingly, in the range $1.42 \leq M \leq 1.67$ oscillations again occur in form of a limit cycle. For $M = 1.42$ it consists of two frequencies, 366 and 609 Hz, being in 3:5 ratio, without any quasi-chaotic components, i.e. the oscillations are purely periodic. For $M = 1.44$ and 1.45, the limit cycle consists of two first natural modes; for higher M it has the first natural mode only. For the latter case, typical reference point deflection, plate shape and spectrum are similar to those shown in Fig. 13. In other words, starting from $M = 1.42$, attractors of the plate motion passes the same stages as before chaotic-like oscillations, but in the reversed order. When increasing Mach number, limit cycle amplitude decreases and becomes almost zero for $M > 1.67$, which means return to stability of the flat state of the plate. This stability retains for higher M until coupled-mode flutter occurs. For the dimensionless flow density $\mu = 8.17 \cdot 10^{-5}$ considered in this study, according to (1) the coupled mode flutter occurs for $M > M_{cr} = 2.92$.

Finally, let us now consider oscillation amplitudes (namely, amplitudes of the reference point) plotted in Fig. 17a. When the plate diverges, starting from $M \approx 0.73$, increase of Mach number yields increase of the divergence amplitude. When passing through $M = 1$, instability converts from divergence to flutter, which is accompanied by a slight drop of the amplitude. Next, when single mode flutter occurs, amplitude increases with increase of M even more rapidly than at divergence. Passing through the region of flutter with internal resonance yields split of the amplitude graph: plate oscillations are non-symmetric so that upper and lower graphs represent higher and lower amplitudes. For the same Mach numbers, single mode limit cycle also exists, which means co-existence of two limit cycles. At $M \approx 1.3$ maximum of amplitude is achieved: $A \approx 0.0038$ m. Further increase of Mach number is accompanied by decrease of the amplitude, and by passing regions of high-frequency periodic and

non-periodic (quasi-chaotic) oscillations. Beyond the region of non-periodic oscillations, oscillation types are passed in the reversed order: high-frequency periodic oscillations, 1:2 resonant limit cycle, and finally first-mode limit cycle. Then the plate returns to the stable state.

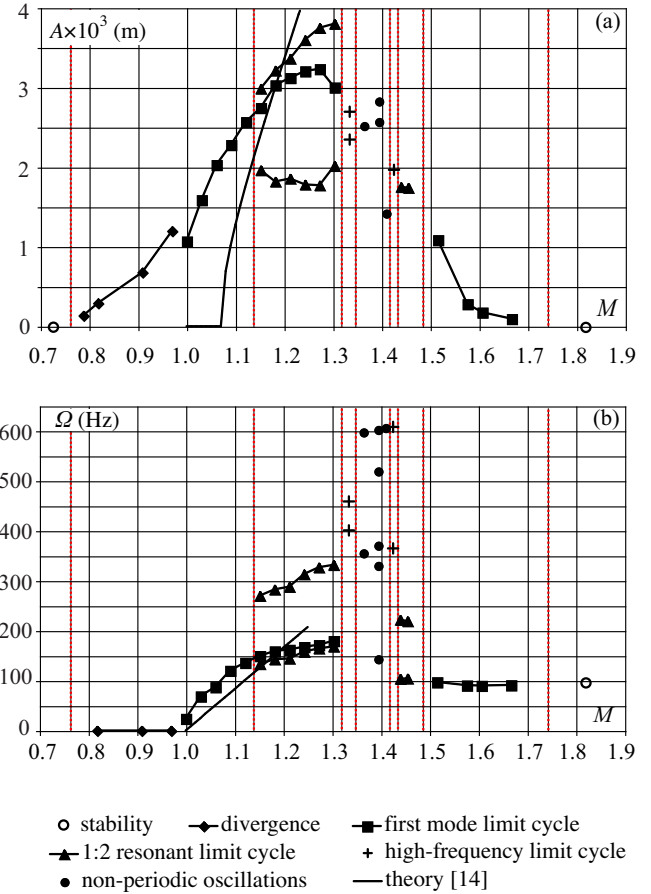


FIGURE 17. AMPLITUDE OF DIVERGENCE AND FLUTTER (a); FREQUENCIES OF SPECTRAL PEAKS (b) VERSUS MACH NUMBER .

Important consequence from Fig. 17a is that typical single mode flutter amplitude is several times higher than that of coupled mode flutter (Fig. 10). This means that single mode flutter can cause fatigue damage much faster, and, hence, it is more dangerous. Region of chaotic-like oscillations is especially dangerous: despite deflection amplitude is of the same order as for single mode limit cycle, plate shape at chaotic oscillations consists of higher natural mode shapes, hence stress amplitude of chaotic oscillations is much higher than that of the single mode limit cycle.

The closed-form solution for single mode flutter amplitude

[14] plotted in the same figure shows the qualitative agreement between the numerical and analytical results. Two quantitative differences are seen: oscillations occur at lower M and grow slower than in [14]. The first difference is caused by the fact that in this study flutter occurs immediately at $M \geq 1$, while analytical theory [14] (not applicable to transonic flows) assumes that it occurs at a slightly higher M . The second difference is due to different plate models (von Karman vs Mindlin plate theory), which yields different plate behaviour at amplitudes of the order of several plate thicknesses. Also, linear aerodynamics was assumed in [14], which is true only for small-amplitude plate oscillations.

Plotted in Fig. 17b are dominating frequencies of spectral peaks (except the triple frequency of the first one: it is caused by cubic plate nonlinearity and is not associated with a separate eigenmode). It is seen that frequency growth in single mode flutter region is almost linear. Frequency of non-resonant limit cycle obtained in a closed-form in [14] is also plotted in Fig. 17b. Results are qualitatively close to each other. When 1:2 internal resonance occurs, frequency growth slows down. After passing through the high-frequency and chaotic regions the frequency and the amplitude decrease.

CONCLUSIONS

Nonlinear development of divergence, single mode and coupled mode flutter of plate have been numerically studied. Amplitudes and frequencies of flutter oscillations have been obtained. In case of high Mach numbers excellent correlation with classical results based on piston theory has been achieved. In case of low supersonic flow four types of flutter oscillations have been observed: first mode limit cycle, limit cycle that includes internal 1:2 resonance, high-frequency periodic oscillations, and non-periodic (quasi-chaotic) plate oscillations. Coupled mode and single mode flutter regions are separated on Mach number axis by a gap, where the plate is stable.

It is shown that amplitude of flutter oscillations at low supersonic Mach numbers is typically higher than that of coupled mode flutter, in accordance with results of [14]. Maximum stress amplitude is achieved at chaotic oscillations and can be much higher than for other flutter types. This is due to higher mode shapes dominating in shape of the plate oscillations.

ACKNOWLEDGMENT

The work is partially supported by Russian Foundation for Basic Research (14-01-31547 and 14-01-00049) and grant NSh-3530.2014.1.

REFERENCES

1. Movchan A.A., 1957, "On Stability of a Panel Moving in a Gas", *Prikladnaya Matematika i Mekhanika*, **21** (2), pp.

- 231–243 (in russian); translated in NASA RE 11-22-58 W,1959.
2. V.V. Bolotin, 1963, *Nonconservative Problems of the Theory of Elastic Stability*, Pergamon Press.
3. Grigolyuk E.I., Lamper R.E., Shandarov L.G., 1965, Flutter of Plates and Shells, *Itogi nauki. Mekhanica*. 1963. Moscow, VINITI, pp. 34-90 (in russian).
4. Dowell E.H., 1974, *Aeroelasticity of Plates and Shells*, Kluwer Academic Publishers.
5. Mei C., Abdel-Motagaly K., Chen R. R., 1999, "Review of Nonlinear Panel Flutter at Supersonic and Hypersonic Speeds", *Applied Mechanics Reviews*, 10, pp. 321–332.
6. V.V. Vedeneev, 2005, "Flutter of a Wide Strip Plate in a Supersonic Gas Flow", *Fluid Dynamics*, 5, pp. 805–817.
7. Vedeneev V. V., 2012, "Panel Flutter at Low Supersonic Speeds", *Journal of Fluids and Structures*, 29, pp. 79–96.
8. Vedeneev V. V., Guvernyuk S. V., Zubkov A. F., Kolotnikov M. E., 2010, "Experimental Observation of Single Mode Panel Flutter in Supersonic Gas Flow", *Journal of Fluids and Structures*, 26, pp. 764–779.
9. Bendiksen O. O., Davis G. A., 1995, "Nonlinear Traveling Wave Flutter of Panels in Transonic Flow", *AIAA Paper 95-1486*.
10. Gordnier R. E., Visbal M. R., 2001, "Computation of Three-Dimensional Nonlinear Panel Flutter", *AIAA Paper 2001-0571*.
11. Hashimoto A., Aoyama T., Nakamura Y., 2009, "Effect of Turbulent Boundary Layer on Panel Flutter", *AIAA Journal*, 47(12), pp. 2785–2791.
12. Aksenov A. A., Dyadkin A.A., Pokhilko V.I., 1998, "Overcoming of Barrier Between CAD and CFD by Modified Finite Volume Method", *Proceedings of 1998 ASME Pressure Vessels and Piping Division Conference*, San Diego, 377-1.
13. Aksenov A., Korenev D., Shishaeva A., Vucinic D., Mravak Z., 2008, "Drop-Test FSI Simulation with Abaqus and FlowVision Based on the Direct 2-way Coupling Approach", *Abaqus Users' Conference*, Newport, Rhode Island, pp. 611-624.
14. V.V. Vedeneev, Limit oscillatory cycles in the single mode flutter of a plate. *Journal of Applied Mathematics and Mechanics* 77 (3) (2013) 257-267.
15. H.G. Schuster, *Deterministic Chaos: An Introduction*, Wiley-VCH, 2005.